

# C3 in UAS as a Means for Secondary Navigation

Jorge Ramirez, Dagoberto Salazar, Xavier Prats and Cristina Barrado

*(Castelldefels School of Telecommunication and Aerospace Engineering, Technical  
University of Catalonia, Barcelona, Spain)*

(E-mail: joraalc@gmail.com)

Unmanned Air Systems (UAS) navigate using Global Navigation Satellite Systems (GNSS), but GNSS vulnerability precludes its use as the only means of navigation and requires a secondary means of navigation. A differentiating characteristic of UAS is their periodic communications with the ground station. This paper analyses the adequacy of employing UAS Command, Control and Communications (C3) as a secondary means of navigation. With no additional infrastructure, an Extended Kalman Filter (EKF) is used to process C3 messages and to obtain the positions of the UAS. Navigation accuracy and integrity are calculated in a scenario with three UAS. The obtained results meet the International Civil Aviation Organization (ICAO) Performance-Based Navigation (PBN) requirements.

## KEY WORDS

1. UAS.
2. Relative Navigation.
3. C3.
4. Secondary Navigation Means.

Submitted: 14 March 2012. Accepted: 28 June 2012. First published online: 29 August 2012.

1. INTRODUCTION. The large number of navigation systems in today's aircraft have motivated studies regarding the integration and fusion of various legacy navigation sources, where different architectures providing fault tolerance are evaluated (e.g., Baraniello and Corrado, 2010). The MITRE Corporation Center for Advanced Aviation System Development presents results from a human-in-the-loop study of cockpit display of traffic information enabled delegated separation, which is based on the availability in the cockpit of the surrounding traffic information (Domino et al., 2010).

Table 1 summarises the accuracies in nautical miles (NM) required by ICAO in the latest version of the Performance-Based Navigation (PBN) Manual (ICAO, 2008). The initial 4 rows (RNAV 10 to RNAV 1) correspond to the accuracies of RNAV (aRea NAVigation) in which the less restrictive value corresponds to the operations over oceanic areas (10 NM). The values of 5 NM and 2 NM are the accuracies that are applicable to the continental and arrival phases, respectively, and the more restrictive accuracy (1 NM) is also applicable to several phases in the approach.

The last 3 rows of Table 1 are the accuracies required to perform operations in Required Navigation Performance (RNP). The main difference between RNAV and

Table 1. Required Accuracy Values (NM, 95% time) and Alarm Limits (NM, Prob =  $10^{-7}$ ).

Navigation Specifications	Flight Phase	Accuracy	Alarm Limit
RNAV 10	En route (oceanic)	10	20
RNAV 5	En route, Arrival	5	10
RNAV 2	En route, Arrival, Departure	2	4
RNAV 1	En route, Arrival, Approach, Departure	1	2
RNP 4	En route	4	8
Basic-RNP 1	Arrival, Approach, Departure	1	2
RNP APCH	Approach (Final)	0.3	0.6

RNP is the requirement in RNP, which is to monitor the on-board performance and send an alert when the performances are not fulfilled (Brooker, 2011). The most stringent case regarding accuracy corresponds to the final phase of the approach, which requires an accuracy of 0.3 NM.

Table 1 also summarises the required alarm values for integrity. The monitoring system will sound an alarm when the calculated confidence level is larger than 20 NM for the RNAV 10 or 10 NM for the RNAV 5 in the case of oceanic operations. The alarm for the approach phase is 0.6 NM, and the most restrictive value for operations in continental airspace is 2 NM.

Global Navigation Satellite Systems (GNSS) provide the positioning accuracy required by the majority of navigation specifications. However, GNSS technology has proven to be vulnerable to interferences to an extent that precludes its use as the only means of navigation (Bonnor, 2012; Volpe, 2001).

The monitoring and alarm capabilities required in RNP regards the concepts of integrity, continuity and availability. This paper evaluates the capacity of the relative navigation concept to provide integrity using the values stated in ICAO (2008). The concepts of continuity and availability are not evaluated in this paper.

The employment of a signal of opportunity as a source for positioning has been a topic of research in various communication scopes. Palmer et al., (2011) proposes the use of a Digital Audio Broadcasting signal for positioning purposes. Ciurana et al., (2006) proposes a methodology for tracking in Wireless Local Area Network locations with Time Of Arrival (TOA) measurements. Qu and Zhang, (2011) propose a methodology to obtain the location of a faulty Unmanned Air Vehicle (UAV) using the communications with the remainder of the UAV in the same multi-UAV flight. This method assumes the capability of obtaining a range of measurements from the other UAV but does not consider the emissions of the other half of Unmanned Air Systems (UAS), i.e., the Ground [control] Stations (GS).

This paper is structured to include a context section, in which this study is introduced through related studies in Section 2, and continues with Section 3 explaining the methodology employed for navigation. The actual simulation performed is described in the Section 4, and the obtained results are explained in Section 5. Finally, Section 6 states the main achievements and identifies several future studies.

2. CONTEXT. Air transportation systems are migrating from using a technology-oriented approach based on legacy systems, to a performance-based

approach in which the performance indicators to be fulfilled by the air transportation system in communication, navigation and surveillance are defined; the support technologies must comply with these indicators. Kerczewski and Kraft, (2006) give an overview of the required performances and the benefits that the performance-based approach could provide. Kozco, (2010) offers an overview of upcoming technologies and their impact on navigation, surveillance and communication. Stroup et al., (2010) analyses the air-ground integration challenges in NextGen identifying the UAS interoperability as a key question for UAS integration.

2.1. *Aeronautical Communications.* EUROCONTROL/FAA, (2007) summarises the recommendations of Eurocontrol and the Federal Aviation Administration for future communications interoperability, assessing several aspects such as the spectrum bands for new systems and identifying the communication roadmap.

A more updated general overview of the current aeronautical communications (mainly based on voice communications), as well as their potential (mainly data-links) to address frequency depletion, is offered by Kamali, (2010).

The compatibility of the legacy aeronautical infrastructure in an L-band with the envisaged physical layer for the aeronautical data-link has been evaluated in Schnell et al., (2010) showing an absence of interference problems when using Time Division Multiple Access (TDMA).

The synchronism mechanisms for the clock of the datalink are not considered in the present study which assumes accuracies of 100 ns, which are in line with existing technologies (Symmetricom, 2009).

2.2. *UAS Communications.* The communications to be employed by UAS are currently under discussion among the involved players in forums such as the EUROCAE WG-73 and the RTCA SC-203, where the contributions to the International Telecommunication Unit conference are decided.

In conventional aviation, communications are performed on-demand. The UAS architecture, with the flight crew displaced to the ground, introduces telemetry and Command and Control (C2), which are required during all the phases of the flight to ensure situational awareness of the flight crew as well as the flight crew's capacity to take control of the flight at any moment.

Currently employed communications in generic UAS are described in Barnard (2007), including an estimation of the data throughput required for the command and status messages, and Barnard proposes a frequency of 4 Hz for the update.

Howell et al., (2010) explains the use of a surrogate aircraft by the NASA (National Aeronautics and Space Administration) Langley Research Center. The evaluated communications resulted in an estimated update frequency of between 3 Hz and 7 Hz, including both uplink and downlink for control.

From an air navigation service provider perspective, Eurocontrol evaluates the saturation of the UAS C2 channel considering different scenarios of UAS deployment with message reporting frequency of approximately 5 Hz (EUROCONTROL, 2010).

Table 2 summarises the data rates proposed in the above-mentioned studies for the UAS datalink. The worst case for navigation purposes is defined by the lowest data rate (1 Hz) because it offers fewer measurements than the other data rates.

3. NAVIGATION METHODOLOGY. We propose a navigation solution using the 2 coordinates of the horizontal plane ( $x, y$ ), as the geometric value of

Table 2. Communication Frequencies (Hz).

Reference	Command and Control (C2)		Telemetry
	Uplink	Downlink	
(Barnard, 2007)	4	4	[1,20]
(Howell et al., 2010)		[3,7]	
(EUROCONTROL, 2010)		5	

$z$  (height) will only occasionally match the value required by aviation (barometric altitude).

3.1. *Problem Statement.* A wireless communication network is assumed based on a TDMA access shared by all of the UAS and GS. The use of a TDMA network provides an explicit knowledge of the time of emission  $t_{e_i}$  of the exchanged messages among  $n$  users. The clock synchronism required by the TDMA allows for the measurement of the TOA  $t_A$  of the message in the same time scale as that of the emitter, i.e., the time shared by the TDMA users.

$$D_i^m = c(t_A - t_{e_i}) \quad (1)$$

However, the real world introduces several errors in  $D_i^m$  that result in pseudo-ranges of the measurements ( $\rho_i$ ). Let  $\rho_i$  be the measured range from an emitter  $i$  located at known coordinates  $(x_i, y_i)$ . If the unknown position of the receiver is  $(x, y)$ , this measured range can be expressed as follows:

$$\rho_i = \sqrt{(x - x_i)^2 + (y - y_i)^2} + c(dt) - c(dt_i) + \epsilon_j \quad (2)$$

where  $c$  is the speed of light.

In fact, the transmitter applies its transmission time pattern with a bias ( $dt$ ). Moreover, the receiver clock measurements will always have a residual clock synchronism bias ( $dt_i$ ); therefore, the actual reception time will be at  $t_i = T + dt_i$ . Finally,  $\epsilon_j$  accounts for all non-modelled propagation factors.

Then, if Equation (2) is linearised around an approximate position  $(x_0, y_0, t_0)$ , we obtain:

$$\rho_i \cong \rho_{i_0} + \frac{x_0 - x_i}{\rho_{i_0}} dx + \frac{y_0 - y_i}{\rho_{i_0}} dy + cdt \quad (3)$$

where  $\rho_{i_0}$  is the approximate range for emitter  $i$ :  $\rho_{i_0} = \sqrt{(x_0 - x_i)^2 + (y_0 - y_i)^2}$ .

Deviations from this approximated position are given by  $dx = x - x_0$ ,  $dy = y - y_0$  and  $cdt$ . Writing the previous equation for all  $n$  emitter measurements in matrix form leads to the following equation:

$$\begin{bmatrix} \rho_1 - \rho_{1_0} \\ \vdots \\ \rho_n - \rho_{n_0} \end{bmatrix} \cong \begin{bmatrix} \frac{x_0 - x_1}{D_{1_0}} & \frac{y_0 - y_1}{D_{1_0}} & 1 \\ \vdots & \vdots & \vdots \\ \frac{x_0 - x_n}{D_{n_0}} & \frac{y_0 - y_n}{D_{n_0}} & 1 \end{bmatrix} \cdot \begin{bmatrix} dx \\ dy \\ dt \end{bmatrix} \quad (4)$$

or, more compactly:

$$Z \cong H \cdot X \quad (5)$$

where, adopting GNSS positioning nomenclature:

$Z$  is the observables vector.

$X$  is the unknown (or state) vector.

$H$  is the geometry matrix.

Note that in GNSS positioning, a single receiver measures the ranges sent by several emitters (satellites). The emitter clock biases are expected to be known (more precisely, are estimated with the information contained in the GNSS navigation message), while the receiver clock bias is the third unknown to be computed along with the receiver position (Parkinson and Spilker, 1996; Hernandez-Pajares et al., 2005).

In our scenario, we also have several network users emitting messages that are employed at the receiver to measure the time of flight. Clock synchronisation is assumed among the network users using high accuracy clocks. The synchronism allows for the measurement of the TOA in a common basis, which is further improved by calculating the clock bias of the receiver as the third variable of the state vector.

A system, such as Equations (4) or (5), is written each time a measurement is performed. In this paper, we propose the use of an Extended Kalman Filter (EKF), aiming at solving the time-evolving Equation (5) that allows the use of the speed and status information transmitted over the network to improve the solution of the equation. The EKF minimises the weighted sum of the squares of the estimation errors, where the weights of each variable are given according to the inverse of the noise variance of the variable (Welch and Bishop, 2001).

Figure 1 summarises the EKF process, in which the estimation of the state vector  $X$  and its associated covariance matrix  $P_X$  are computed at each iteration of the filter, combining the following:

- A prediction obtained from the previous state with a transition matrix ( $A$ ) and a process noise ( $Q$ ).
- The measurements  $Z$  and the associated updates on the measurement noise ( $P_Y$ ) and the geometry (or measurement) matrix  $H$ .

3.2. *Confidence Level.* ICAO defines the cross track error ( $e_{ct}$ ), in ICAO, (2008), as the minimum distance from the actual point to the trajectory. The proposed EKF calculates the UAV position in a Cartesian space with North and East as the reference frame.

Defining  $e_{ct}$  as the magnitude related to the directional components of the error ( $e_x, e_y$ ), we assume that a Rayleigh distribution can be observed. Equation (6) shows the cumulative distribution function (CDF) of the Rayleigh distribution for a variable  $x$ :

$$F(x) = 1 - e^{-\frac{x^2}{2\sigma^2}} \quad (6)$$

where:

$$x = \sqrt{-\ln(1 - F(x))2\sigma^2} \rightarrow x = \sigma\sqrt{-2\ln(1 - F(x))} \quad (7)$$

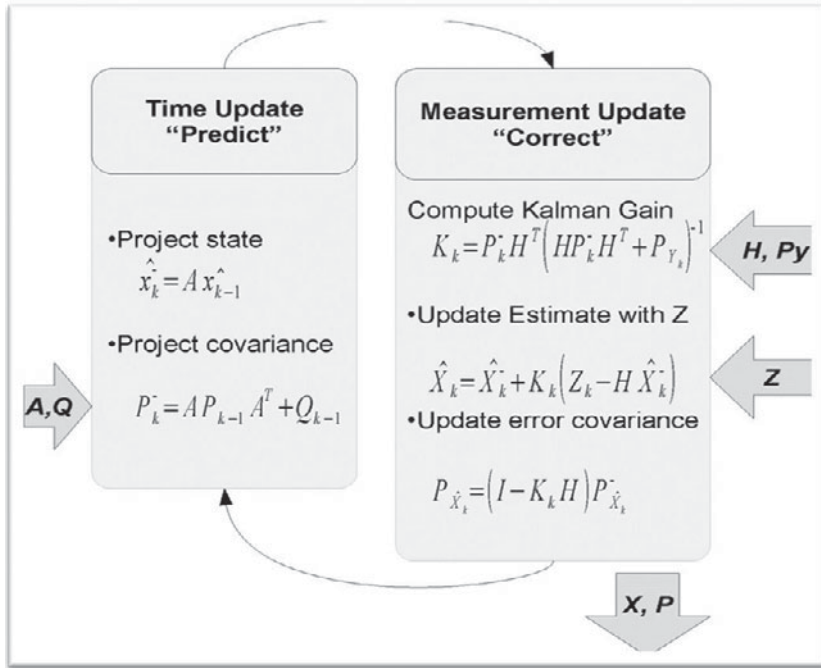


Figure 1. Extended Kalman Filter.

Next, a confidence interval of  $1-10^{-7}$ , as required by ICAO, is obtained for a value of  $\approx 5, 6777$  times the  $\sigma$  of the error distribution. Because the exact distribution of the error is unknown, the protection level equations stated in Appendix J of RTCA, (2006) are applied to obtain an over-bound of the real  $\sigma$ .

$$d_{major} = \sqrt{\frac{d_{east}^2 + d_{north}^2}{2} + \sqrt{\left(\frac{d_{east}^2 - (d_{north}^2)}{2}\right)^2 + d_{en}^2}} \quad (8)$$

Equation (8) defines the  $\sigma$  to be employed in Equation (7) ( $d_{major}$ ) as a combination of several values of the law of the propagation of errors, as indicated in Equation (9). In the Global Positioning System (GPS) positioning, the concept of Dilution of Precision uses the law of the propagation of errors to estimate the confidence level that the positioning could offer in the same coordinate frame (Langley, 1999).

$$(H^T \cdot W \cdot H)^{-1} = \begin{bmatrix} d_{east}^2 & d_{en} & d_{et} \\ d_{ne} & d_{north}^2 & d_{nt} \\ d_{te} & d_{tn} & d_{time}^2 \end{bmatrix} \quad (9)$$

Equation (9) provides the covariance along the diagonal for each component (East, North and time) and the correlation between the variables outside the diagonal that propagated from each measure using the User Equivalent Range Error (UERE) due to the geometry of the problem ( $H$ ). The weighted matrix required in Equation (9) is defined in Equation (10). It is a diagonal matrix with the square of the inverse of the

UERE value for each measure:

$$W = \begin{bmatrix} \frac{1}{\sigma_1^2} & 0 & \dots & 0 \\ 0 & \frac{1}{\sigma_2^2} & \dots & 0 \\ \vdots & \vdots & \ddots & \vdots \\ 0 & 0 & \dots & \frac{1}{\sigma_n^2} \end{bmatrix} \quad (10)$$

$$HPL = K \cdot d_{major} \quad (11)$$

It should be noted that the Horizontal Protection Level (HPL) calculated in Equation (11) represents an upper bound for the  $\sigma$  of the positioning error as the considered error depends on the direction of the trajectory; therefore, the estimated HPL depends on the geometry of the different measures employed.

4. SIMULATION. The envisaged simulation attempts to evaluate the performance of a secondary means of navigation on the basis of the C3 communications between a UAV and its GS, which operates from a static position.

A fault-free navigation position is calculated as a result of the distance measurements between the target and the other users. Assuming that the primary navigation mean (GPS) positioning is not available at the target, the positions of the remaining users are obtained from their GPS and are propagated through a TDMA-based network in which the communicating nodes (UAV and GS) are capable of maintaining the synchronisation of their clocks with a common time basis.

To provide a realistic assessment of the accuracy and integrity that relative navigation could offer, a scenario has been simulated with three UAS flying simultaneously significant trajectories of existing aerial works for a period of 24 hours. UAS communicates with their respective GS with 1-s communication latencies and 100-ns clock accuracies.

4.1. *Vehicles Trajectories.* While a rich scenario could be envisaged in a metropolitan area, a reduced subset of meaningful UAS operations has been selected as the trajectories to be simulated:

- Traffic monitoring: [Figure 2a](#).
- Lifeguard supervision of the coastline: [Figure 2b](#).
- Vineyard monitoring: [Figure 2c](#).

A trajectory similar to several of the main motorways surrounding Barcelona has been simulated in [Figure 2a](#). The motorways connecting Barcelona with the major Spanish cities as well as the European motorways have not been considered. The entire flight has been simulated at a constant speed of 40 m/sec.

A lifeguard flight has been simulated in [Figure 2b](#). Although almost the entire coastline of Catalonia has significant beaches, only the monitoring of a small portion

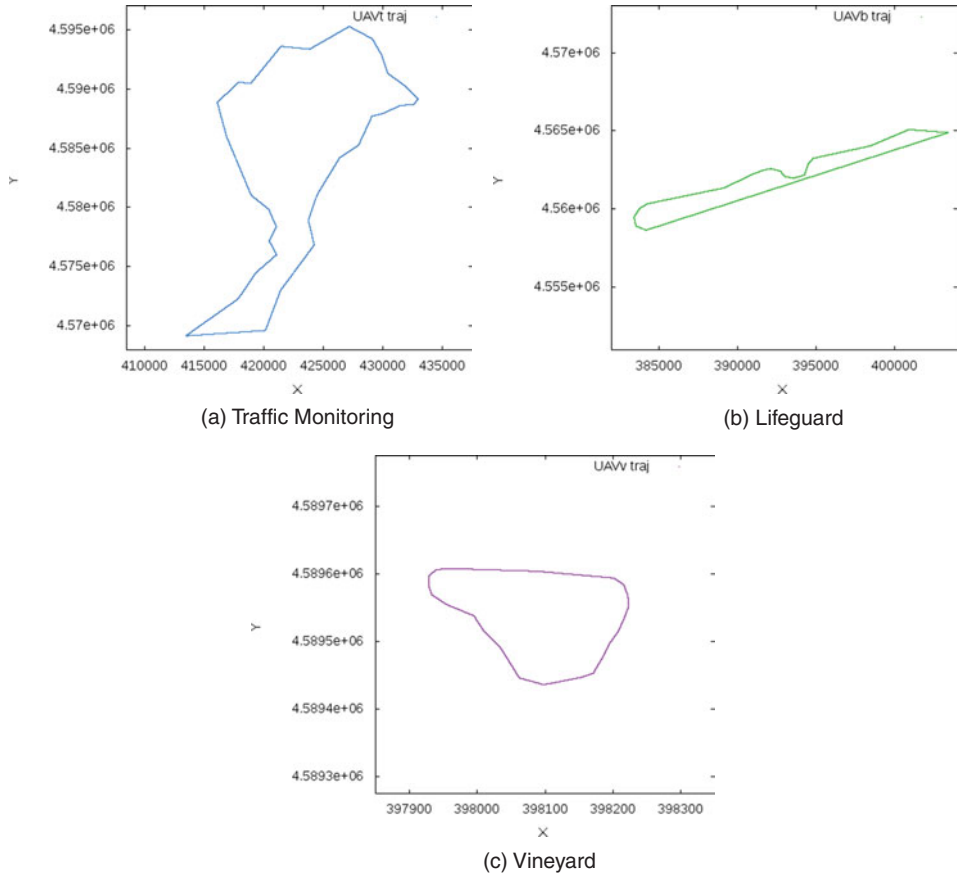


Figure 2. Simulated Trajectories.

of the coastline has been simulated. The entire flight has been simulated at a constant speed of 20 m/sec.

A small vineyard monitoring flight has been simulated in Figure 2c. Despite the large area of vineyards that exist in Catalonia, only a small vineyard monitoring flight has been simulated. The entire flight has been simulated at a constant speed of 10 m/sec.

Figure 3 shows the relative positions of the GS and the flight paths. The green triangle represents the location of the GS that controls the lifeguard UAV (trajectory in green). The magenta triangle represents the position of the GS that controls the UAV performing agricultural air works in the vineyard (trajectory in magenta). Finally, the blue triangle placed on the coastline of Barcelona represents the GS of the UAV monitoring the traffic of the metropolitan area of Barcelona.

#### 4.2. Communications.

4.2.1. *Visibility.* Table 3 summarises the selected static model of visibility between the UAV and the GS. Sub-indexes  $t$ ,  $l$  and  $v$  stand for traffic, lifeguard and vineyard, respectively.

In the reduced visibility scenario ( $\surd$ ), each UAV could see the other UAVs and its own GS as a minimum. Additionally,  $UAV_t$  could see  $GS_l$ , and  $UAV_l$  could see  $GS_v$ .



Table 3. Visibility.

Listener	Emitter					
	$UAV_t$	$GS_t$	$UAV_l$	$GS_l$	$UAV_v$	$GS_v$
$UAV_t$		✓	✓	✓	✓	†
$UAV_l$	✓	✓		✓	✓	†
$UAV_v$	✓	†	✓	†		✓

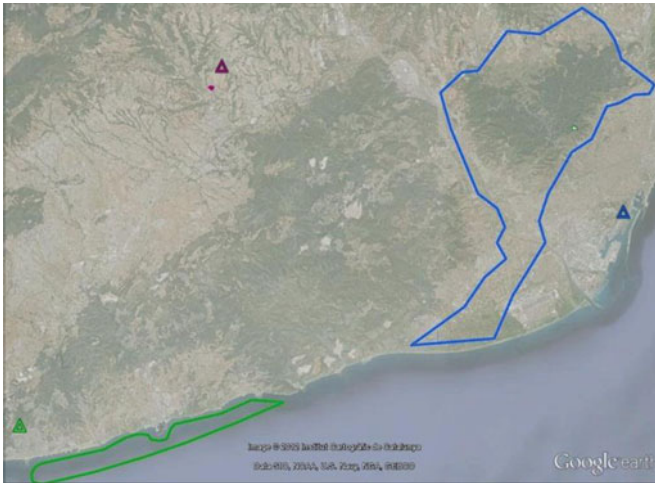


Figure 3. Flight test and Ground Stations (GS) simulated.

The visibility model summarised in Table 3 does not take advantage of all the available transmission-to-measurement distances, discarding accurate measurements from the static positions. In the case of  $UAV_t$  and  $UAV_l$ , the discarded measurements correspond to  $GS_v$ .

In the case of  $UAV_v$ , the measurements from  $GS_t$  and  $GS_l$  are discarded, retaining two mobile references  $UAV_t$  and  $UAV_l$  and the flight’s individual  $GS_v$  as the only static reference.

A slightly improved visibility model (✓ plus †) is also simulated to assess the effect of adding measures to the equation system. The listener has the capability to receive the messages sent by any of the other users. The number of measures ranges from 4 to 5 for  $UAV_t$  and  $UAV_l$ , respectively, and in the case of  $UAV_v$ , the number of measures ranges from 3 to 5.

4.2.2. *Proposed Messages.* The EKF is improved with additional information available inside the C3 messages as follows:

- Position Report.
- Speed Vector.
- Clock Bias.

The self-positions of the remaining users are known at each position (air and ground) from GPS. As part of the C3 messages, they will share their new position every second.

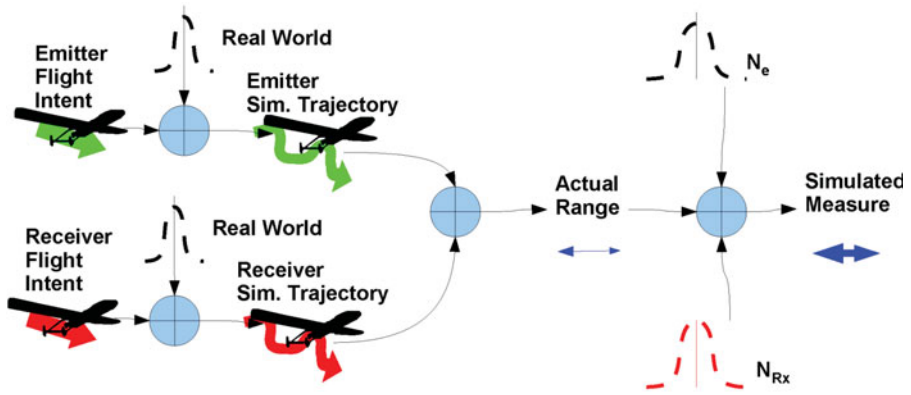


Figure 4. Measurement Generation.

The speed of each aircraft can be retrieved from GPS but also from other sources, such as the inertial systems or a combination of the compass and the speedometer. We will assume that the speed is given as a three-dimensional vector ( $x$ ,  $y$ , and  $z$ ). The GS will not report any speeds. Time measures and corrections are a significant part of the EKF. The calculated time corrections should be interpreted as the clock bias between the receiver clock and the common network clock. We will assume that each aircraft and ground station will calculate and propagate its own calculated clock bias. This approach will result in our obtaining an estimation of the clock bias of each network user as part of the EKF inputs.

Finally, we will assume that all three data types (position, speed and clock) are packed in the same message in the low bandwidth scenario (one message per second) defined in Section 2.2, rather than increasing the number of messages and eventually the frequency of communication.

4.3. *Measures Generation.* The navigation accuracy of the proposed algorithm is verified using a simulated set of measurements obtained from the different trajectories, as shown in Figure 4, and the results are compared with the actual position to test the proposed accuracy. To obtain each measurement range, the next steps in the simulation are as follows:

The intended position of the emitter and the receiver are computed.

Both the intended positions of the emitter and the receiver are modified with a zero mean and a normally distributed noise, with  $\sigma=10$  m for  $x$  and  $y$ , and  $\sigma=2$  m for  $z$ . The resulting simulated positions reflect the imperfection of the trajectory in the real world.

These simulated positions are used to compute the actual range.

The actual range is modified by adding a synchronism noise ( $N_{synch}$ ) that is introduced by the emitter ( $N_e$ ) and the receiver ( $N_{Rx}$ ).

Equation (12) shows how  $N_{synch}$  is composed of the error between the emitter and the reference time.  $dt_{synch}$  is simulated with an initial value that is normally distributed with a zero mean and a standard deviation of 100 ns. Both the ageing component and the noise defined by the Allan variance are added to the initial value. Considering  $c$ ,  $N_{synch}$  has values fewer than 30 m 68% of the time.

$$N_{synch} = c * dt_{synch} \quad (12)$$

4.4. *EKF Instantiation.* As shown in Figure 1, EKF requires the definition of  $A$ ,  $Q$ ,  $H$ ,  $P_Y$  and  $Z$  for each iteration.

4.4.1. *'A' Dynamic Model.* Because the navigation methodology proposed in this paper benefits from a large number of fairly reliable measures ( $Z$ ), the dynamic behaviour of the UAV and the  $(x, y)$  coordinates can be simply modelled as a kinematic process (Hernandez-Pajares et al., 2005). Accounting for the above considerations, the transition matrix can be written as follows:

$$A = \begin{pmatrix} 0 & & \\ & 0 & \\ & & 0 \end{pmatrix} \quad (13)$$

4.4.2. *'Q' Process Noise.* Equation (14) shows the proposed process noise matrix:

$$Q = \begin{pmatrix} \dot{q}_x \Delta t & & \\ & \dot{q}_y \Delta t & \\ & & (c\sigma_{\varepsilon_{synch}})^2 \end{pmatrix} \quad (14)$$

where:

$\Delta t$  is the time between two consecutive samples.

$\dot{q}_j = \frac{d\sigma_j^2}{dt}$  is the spectral density of coordinate  $j$ , which is defined by a random process ( $j = \{x, y\}$ ).

$\sigma_{\varepsilon_{synch}}$  is the standard deviation of the synchronism error of the clock.

$\dot{q}_j = \frac{d\sigma_j^2}{dt}$  takes on the values of the known individual speeds.

The calculation of the clock bias simplifies  $\sigma_{\varepsilon_{synch}}$  to the Allan deviation  $\sigma_A$  because  $C_{Ag}$  has a tendency to be slow enough to be absorbed in the value of the clock bias. Then, the calculated clock bias is the sum of  $C_{Ac}$  and  $C_{Ag}$ , with  $\sigma_A$  as the clock source of error for the process.

4.4.3. *'H' Geometry Matrix.* As seen in Equation (4), each row of the geometry matrix  $H$  is defined as  $\frac{x_0 - x_i}{D_{i0}} \frac{y_0 - y_i}{D_{i0}}$ , where  $(x_0, y_0)$  defines the estimation of the individual position, and  $(x_i, y_i)$  defines the position of the emitter.

Each time that an incoming message is employed for measuring a distance, it is calculated through an iteration of the EKF and the time employed since the last measuring ( $\Delta t_{meas}$ ) is calculated as well as the time since the position of each network user was last reported ( $\Delta t_{rep_i}$ ).

The individual position  $(x_0, y_0)$  is obtained from the last position calculated  $(x_0^-, y_0^-)$  by adding the displacement, as in Equation (15), where  $(Sp_{x_0}, Sp_{y_0})$  is the individual speed and  $\Delta t_{meas}$  is the time since the last measurement.

$$\begin{pmatrix} x_0 \\ y_0 \end{pmatrix} = \begin{pmatrix} x_0^- \\ y_0^- \end{pmatrix} + \begin{pmatrix} Sp_{x_0} \\ Sp_{y_0} \end{pmatrix} \Delta t_{meas} \quad (15)$$

The emitter's position  $(x_i, y_i)$  is obtained from the last position reported  $(x_i^-, y_i^-)$  by adding the displacement, as in Equation (16), where  $(Sp_{x_i}, Sp_{y_i})$  is the reposted speed and  $\Delta t_{rep}$  is the time elapsed since the position of the emitter was reported.

$$\begin{pmatrix} x_i \\ y_i \end{pmatrix} = \begin{pmatrix} x_i^- \\ y_i^- \end{pmatrix} + \begin{pmatrix} Sp_{x_i} \\ Sp_{y_i} \end{pmatrix} \Delta t_{rep_i}. \quad (16)$$

4.4.4. *'P<sub>Y</sub>' Measurement Noise.* The measurement covariance matrix is modelled in this problem as:

$$P_Y = \begin{pmatrix} \sigma_1^2 & & \\ & \ddots & \\ & & \sigma_n^2 \end{pmatrix} \quad (17)$$

If we consider the different sources of error as independent, then they can be root-sum-squared to obtain a value for  $\sigma$ . This value is known in GPS as the 'UERE'. Then, the UERE to be applied for each measure of distance from an emitter  $i$  is the sum of all of the covariance of the individual sources of error (Equation 18):

$$\sigma_i^2 = \sigma_{clk_i}^2 + \sigma_{clk_r}^2 + \sigma_{v_i}^2 + \sigma_{v_r}^2 + \sigma_{trop}^2 + \sigma_{mult}^2, \quad (18)$$

where:

The variances of the error generated by the clock synchronism error of the emitter  $\sigma_{clk_i}^2$  and the receiver  $\sigma_{clk_r}^2$  are defined using the Allan deviation  $\sigma_A$  of the envisaged clocks multiplied by  $c$  (Symmetricom, 2009).

The covariance of the emitter position  $\sigma_{v_i}^2$  and the receiver position  $\sigma_{v_r}^2$  are defined using the declared accuracy performance of EGNOS in (ESA, 2009). If the troposphere effect on the signal transmission has not been simulated, then the value of  $\sigma_{trop}^2$  is assigned as 0. The multipath effect on the signal transmission has not been simulated and, consequently, the value of  $\sigma_{mult}^2$  is assigned as 0.

4.4.5. *'Z' Measures Refinement.*  $Z$  is defined as the difference between the pseudo-range and the distance estimation ( $\rho_i - \rho_{i_0}$ ). The accuracy of  $\rho_i$  is improved when applying Equation (1) due to the knowledge of individual clock bias, which has been calculated, and by the knowledge of the emitters' clock bias, which has been reported through the network.

In contrast, the  $\rho_{i_0}$  accuracy is improved as a result of the increased knowledge of  $(x_0, y_0)$  and  $(x_i, y_i)$  presented by Equations (15) and (16).

5. RESULTS. The EKF of Section 3.1 is instantiated as explained in Section 4 for each trajectory, i.e., each trajectory has its own exclusive EKF to calculate positioning. The obtained position is compared with the actual position, and the along-track error ( $e_{at}$ ) and the cross-track error ( $e_{ct}$ ) are calculated. The simulations are performed with the low visibility scenario defined by Table 3.

The  $e_{ct}$  is compared with the confidence level calculated, as described in Section 3.3, providing an assessment of the integrity of the navigation. The simulations are performed with the low visibility scenario defined by Table 3, and the case with the worst integrity is compared against itself simulated with a slightly improved visibility scenario defined by Table 3.

5.1. Accuracy. Both  $e_{at}$  and  $e_{ct}$  are compared with the ICAO performance navigation accuracy required values of Table 1 in Section 1. The listed values are the upper values and must not be exceeded more than 5% of the time to be considered acceptable.

5.1.1. Along-Track Error. Figures 5a, 5b and 5c show the  $e_{at}$  values of the navigation solution. Both the lifeguard (Figure 5b) and vineyard (Figure 5c) trajectories allow the error to be distributed under 40 m. The traffic monitoring,

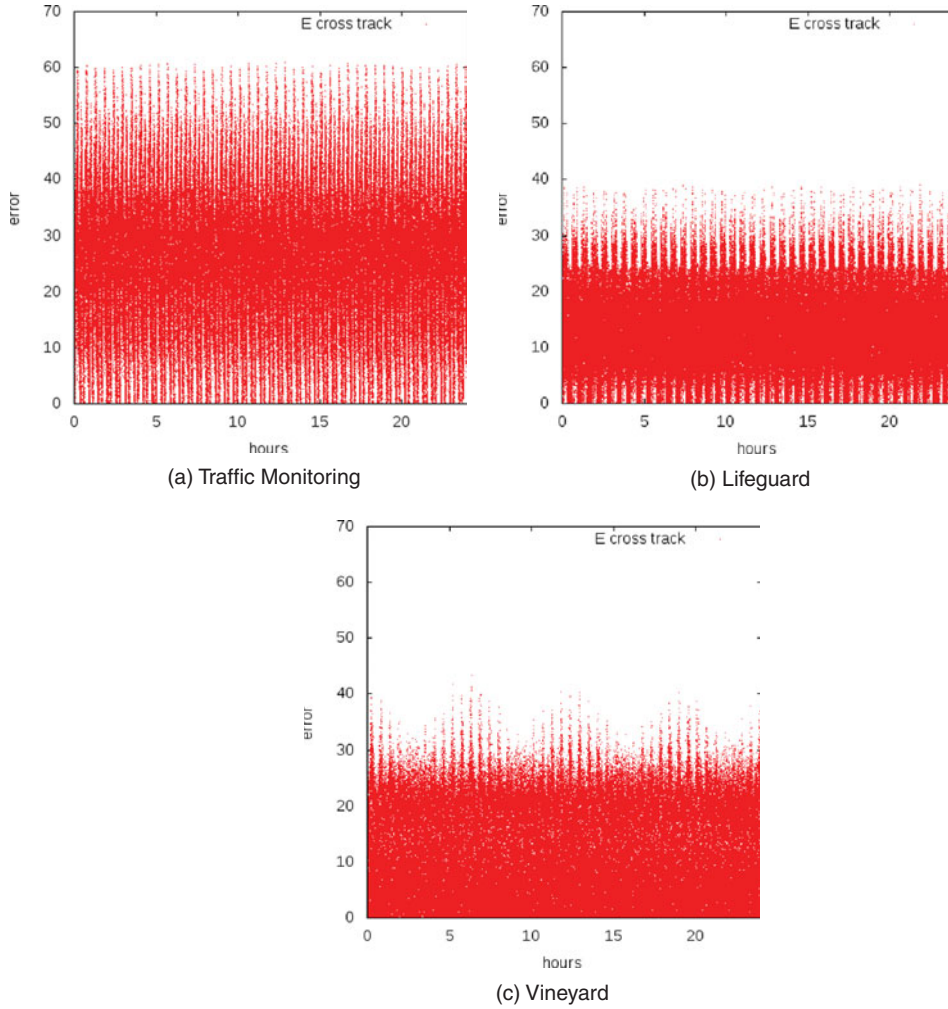


Figure 5. Along-Track Errors.

which has a more exigent trajectory and a faster speed, increases its error threshold up to 60 m.

Figures 6a, 6b and 6c show the histograms of the error. The traffic monitoring error has the greatest mean and standard deviation.

Table 4 summarises the basic statistics of the along-track error module. Traffic monitoring has an along-track mean  $\bar{e}_{at}$  of 25.87 m with a standard deviation  $\sigma_{e_{at}}$  of 20.65 m.

Using the Rayleigh CDF of Equation (7), the required 95% accuracy is achieved at a value of 50.55 m for the worst case (traffic monitoring), which is in fact sufficient to comply with the most restrictive navigation specification. For the case of the lifeguard and the vineyard trajectories, their lower value of  $\sigma_{e_{at}}$  also ensures compliance with the stringent navigation specifications (RNP APCH).

5.1.2. Cross-Track Error. Figures 7a, 7b and 7c show the  $e_{ct}$  values in the simulation. Both the lifeguard (Figure 7b) and vineyard (Figure 7c) trajectories allow

Table 4. Along-Track Error Accuracy Statistics.

Statistic	Trajectory		
	Traffic	Lifeguard	Vineyard
$\bar{e}_{at}$	25.87	12.99	12.09
$\sigma_{e_{at}}$	20.65	9.94	9.27
$CDF_{e_{at}} (95\%)$	50.55	24.33	22.69

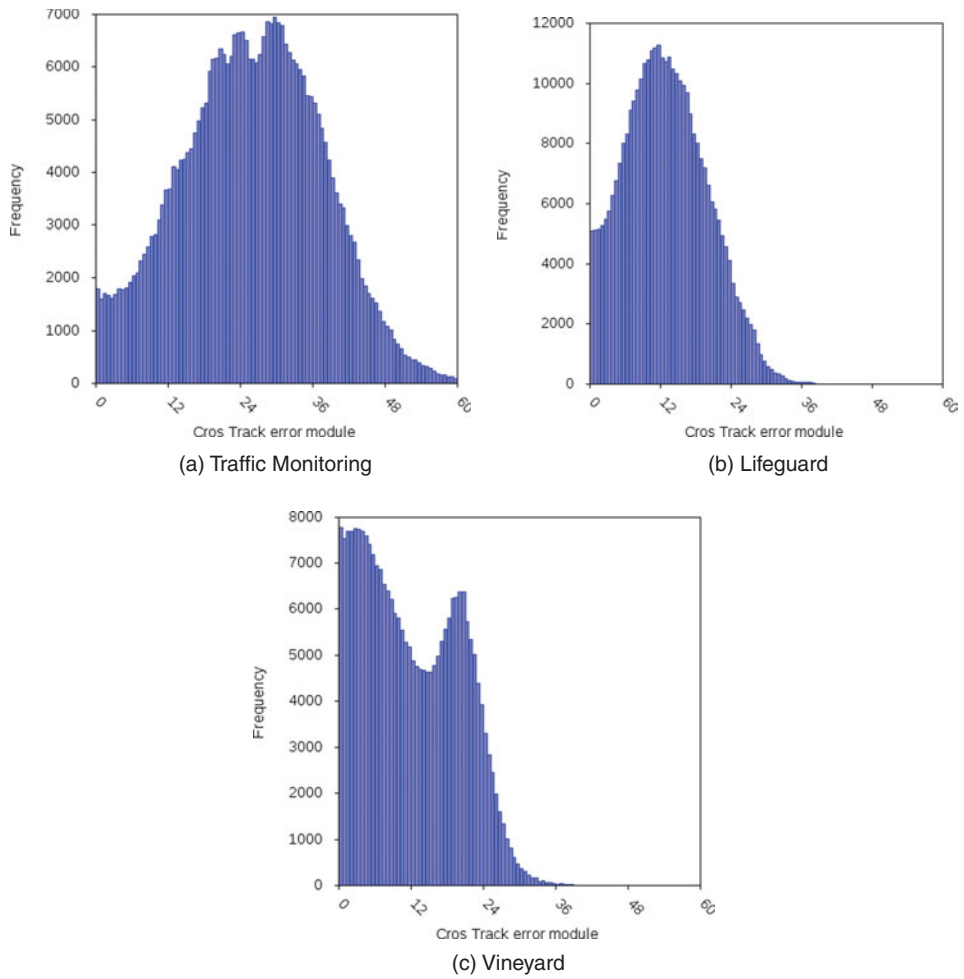


Figure 6. Along-Track Frequencies.

the error to be distributed under 20 m. The traffic monitoring scenario, which is the worst case, has an increased error threshold up to 30 m.

Comparing  $e_{at}$  (Figure 5) with  $e_{ct}$  (Figure 7), we could appreciate the better behaviour in the cross-track direction relative to the along-track direction.  $e_{ct}$  is interpreted in aviation as trajectory abandonment, which is more sensitive in aviation than a delay

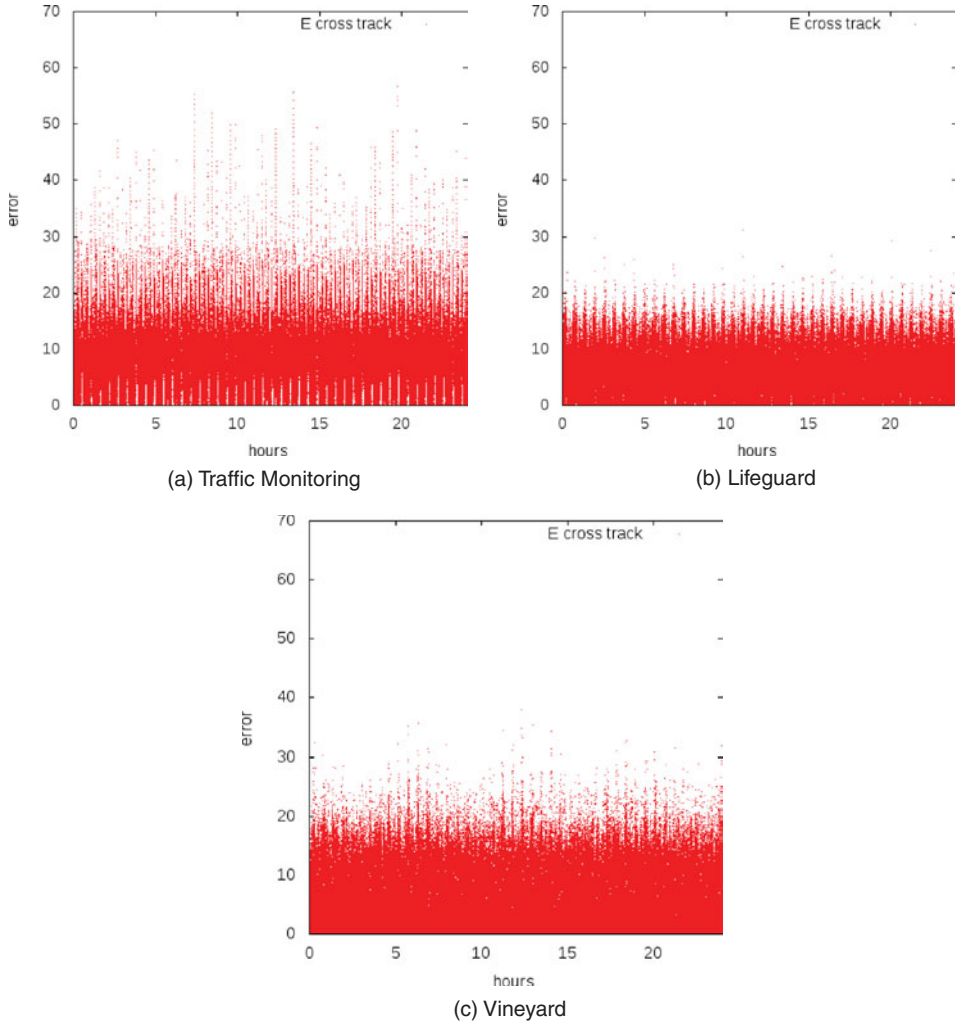


Figure 7. Cross-Track Errors.

or a time advance, which are the interpretations of  $e_{at}$ . Therefore, the most sensitive direction benefits from a better accuracy, which is offered by the proposed EKF.

Figures 8a, 8b and 8c show the histograms of the error, and Table 5 shows the statistical values.

The worst case in Table 5, the traffic monitoring trajectory, has a mean error  $\bar{e}_{ct}$  of 8.78 m and a standard deviation  $\sigma_{e_{ct}}$  of 5.81 m. Using the Rayleigh CDF of Equation (7), the required 95% accuracy is achieved at a value of 14.22 m for the worst case (traffic monitoring), which is (as for  $e_{at}$ ) sufficient to comply with the RNP APCH. For the case of the lifeguard and the vineyard trajectories, with a lower  $\sigma_{e_{ct}}$  the compliance with RNP APCH is also improved.

Comparing the values of  $CDF_{e_{ct}}(95\%)$  and  $CDF_{e_{at}}(95\%)$  trajectory by trajectory, the improvement in the accuracy of the cross-track error could be observed, which in fact is most critical between  $e_{at}$  and  $e_{ct}$ .

Table 5.  $e_{ct}$  Accuracy Statistics.

Statistic	Trajectory		
	Traffic	Lifeguard	Vineyard
$\bar{e}_{ct}$	8.78	5.89	7.27
$\sigma_{e_{ct}}$	5.81	3.96	5.25
$CDF_{e_{ct}}(95\%)$	14.22	9.69	12.85

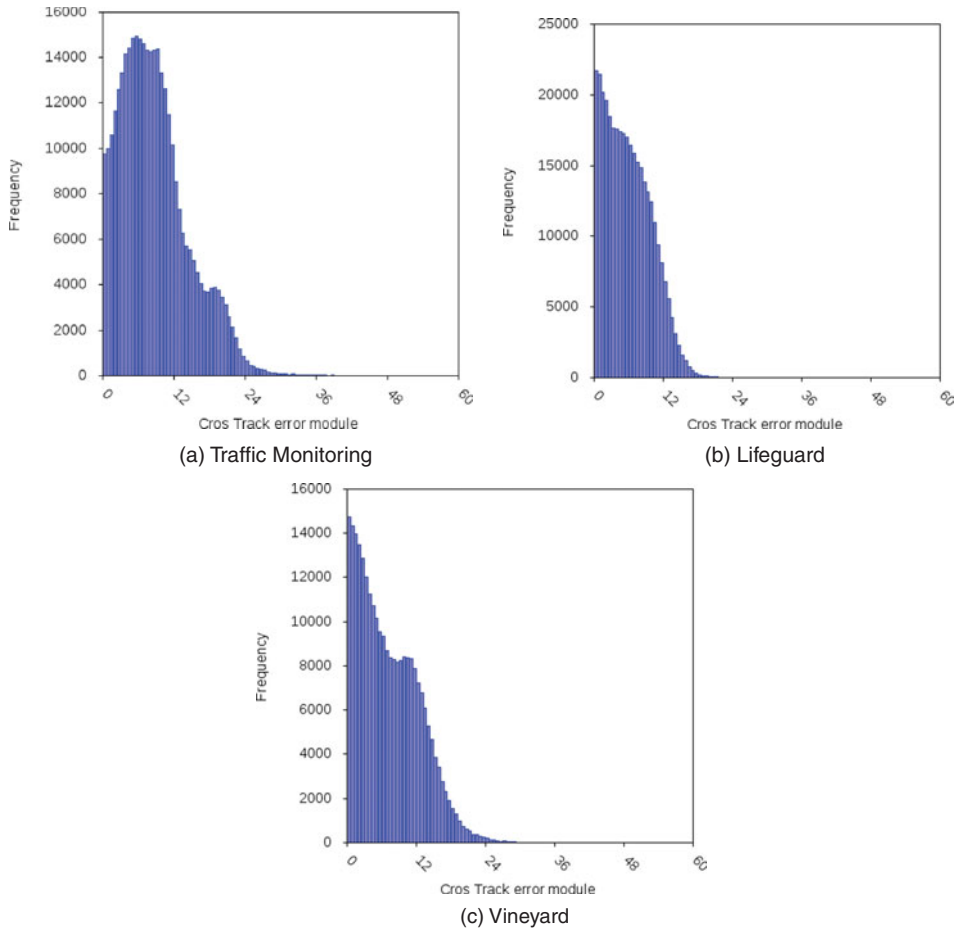


Figure 8. Cross-Track Frequencies.

5.2. Integrity. The confidence level is calculated as explained in Section 3.3 and compared with the actual error by displaying them in the same figure. The compliance is assessed with the integrity requirements stated in Table 1 of Section 1.

5.2.1. Reduced Visibility. Simulating the relative navigation with the reduced visibilities stated in Table 3 the confidence levels of Figures 9a, 9b and 9c are obtained.

Figure 9c shows how the  $UAV_v$  achieves the lowest confidence level. This is a consequence of the better geometry of the emitters employed compared with the



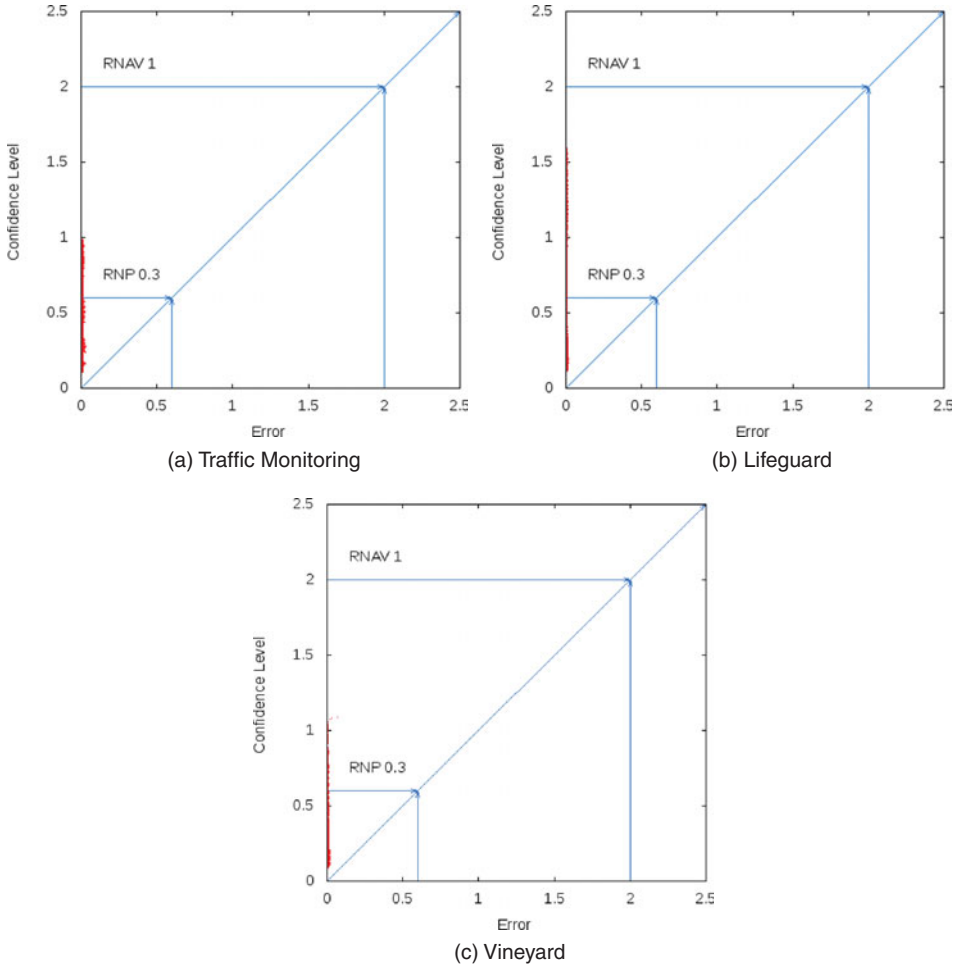


Figure 9. Confidence Levels.

geometry of the emitters employed at the remaining trajectories. Figure 9a shows how the traffic monitoring scenario benefits from the better geometry of the employed emitters than the lifeguard UAS. The confidence level of the traffic monitoring trajectory is lower than the confidence level of the lifeguard trajectory, and the inverse relationship is true for the accuracy values in which the lifeguard trajectory (Figure 7b) has better values than the traffic monitoring trajectory (Figure 7a).

The integrity values obtained do not achieve the required values for RNP APCH but comply with the RNP 1 navigation specifications.

Table 6 shows the compliance of the different trajectories with the navigation specifications. Although all of the trajectories comply with RNAV 1 for 100% of the time, compliance with RNP APCH could serve as a numeric indicator of the sufficiency of the confidence level. Using the percent-compliance values with RNP APCH, it could be observed that the vineyard trajectory has the best compliance value of 99.2%, followed by the lifeguard trajectory with an 88.3% compliance and finally, the traffic monitoring trajectory with an 82.6% compliance. Nevertheless, in Figures

Table 6. Integrity Alarm Values Compliance.

Navigation Specifications	Trajectory		
	Traffic	Lifeguard	Vineyard
RNAV 1	1	1	1
Basic-RNP 1	1	1	1
RNP APCH	0.826	0.883	0.992

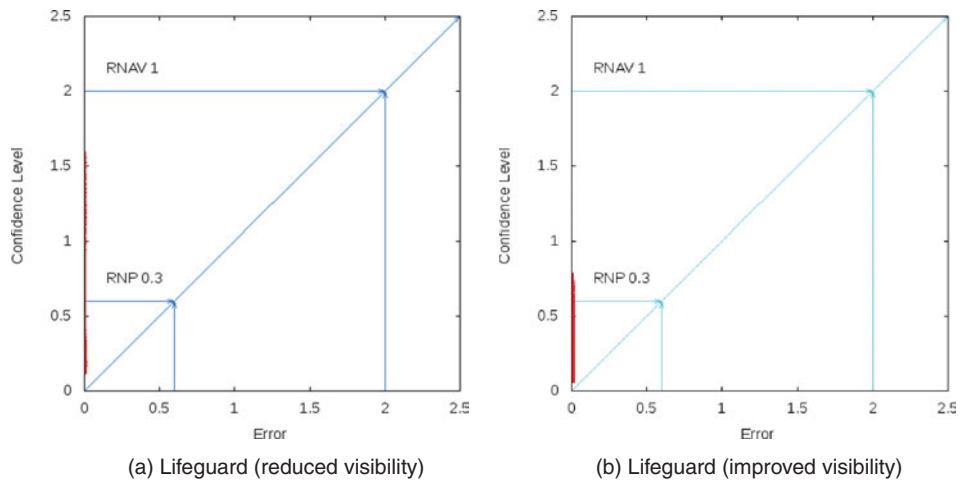


Figure 10. Confidence Level Improvement.

9a and 9b, it could be observed that the tail approaches the upper values in the case of the lifeguard trajectory, which has better compliance values with RNP APCH.

5.2.2. *Improved Visibility.* When the confidence values that are achievable with the visibilities shown in Table 3 are accessed, an improved version of the communications can be simulated to assess the effect on the confidence level of a richer scenario.

Figure 10 shows how the confidence values are improved from Figure 10a (reduced visibility of Table 3) to Figure 10b (improved visibility of Table 3).

Table 7 shows how the confidence level is dramatically improved from the standard scenario in which the compliance with RNP APCH is 88.3% to the improved scenario in which the value of compliance is increased to 96.6%.

6. CONCLUSIONS. This paper presents a relative navigation solution for Unmanned Air Systems (UAS) that can be used as a secondary means of navigation.

UAS normal operation depends on frequent Command and Control (C2) messages sent from vehicles to ground stations and vice versa. The navigation solution we propose only uses these messages. No additional resources (new infrastructures or additional radio frequencies) are required. Thus, this secondary navigation solution is cost effective. The proposal assumes that UAS communicate using a Time Division Multiple Access (TDMA) network. The message's Time Of Arrival (TOA) is used to

Table 7. Improvement in Integrity Alarm Value Compliance.

Navigation Specifications	Trajectory	
	Lifeguard	Improved Lifeguard
RNAV 1	1	1
Basic-RNP 1	1	1
RNP APCH	0.883	0.966

calculate the distance between the receiver and the emitter. All distance measures are refined using an Extended Kalman Filter (EKF). The information of the messages is used for this refinement. In our proposal, all messages contain the position, speed and clock bias of the emitter.

Accuracy results are always within 1 NM i.e., RNAV 1 (aRea NAVigation) and RNP 1 (Required Navigation Performance) compliant for a simulated scenario, with only 3 UAS and 1 message per second and per emitter. The mean accuracy values are in the range of 5 m to 26 m, and the worst case has a 60 m along-track error. In the same simulation, the confidence levels are also calculated. All of the confidence level values are compliant with the RNP 1 integrity requirements.

We conclude that a UAS can navigate in the most stringent RNP airspace even when losing the Global Navigation Satellite Systems (GNSS) signal using the C2 signals of the other UAS. Utilising more than 3 UAS and/or higher frequencies of C2 messages are reasonable scenarios that will further improve the accuracy and integrity values presented.

In the near future, UAS will become frequent users of non-segregated airspace. More UAS communications represent more signals of opportunity. This increase will provide better navigation accuracy and integrity not only to UAS but also to conventional aircraft. Any airspace user can use this backup navigation method with a very good accuracy, with only a low cost radio receiver listening on the UAS frequency. In addition, as an example of communication / navigation / surveillance integration, ground surveillance tasks will benefit from UAS communications using the proposed model.

Future work includes:

- Modelling multi-path and troposphere effects in the EKF.
- Studying a scenario where all UAS lose GNSS navigation at the same time.
- Improving ground station geometry by adopting a more peripheral distribution.
- Or, obtaining accuracy measures for scenarios in which UAS and conventional aircrafts share airspace.

## ACKNOWLEDGEMENTS

This work has been co-financed by the Ministry of Science and Education of Spain under contract CICYT TIN 2010-18989. This work has also been co-financed by the European Organization for the Safety of Air Navigation (EUROCONTROL) under its CARE INO III program. The content of the work does not necessarily reflect the official position of EUROCONTROL on the matter.

## REFERENCES

- Baraniello, V. R. and Corrado, F. (2010). Unconventional Integrated Navigation Systems Based on Redundancy of Traditional Navigation Sensors. *Proceedings of AIAA Guidance, Navigation and Control Conference*, Toronto, Ontario, Canada.
- Barnard, J. (2007). Small UAV Command, Control and Communication Issues. *Proceedings of Communicating with UAV's, 2007 IET Seminar on*, Savoy Place, London, UK.
- Bonnor, N. (2012). A Brief History of Global Navigation Satellite Systems. *The Journal of Navigation*, **65**, 1–14.
- Brooker, P. (2011). Air Traffic Control Separation Minima: Part 2 Transition to a Trajectory-based System. *The Journal of Navigation*, **64**, 673–693.
- Ciurana, M., Barcelo, F. and Cugno, S. (2006). Indoor Tracking in WLAN Location with TOA Measurements. *MobiWac06*, Torremolinos, Malaga, Spain.
- Domino, D. A., Tuomey, D., Mundra, A. and Smith, A. (2010). Air Ground Collaboration Through Delegated Separation: Application for Departure and Arrivals. *Proceedings of Integrated Communications Navigation and Surveillance Conference (ICNS), 2010*, Herndon, VA, USA.
- ESA. (2009). *EGNOS: European Geostationary Navigation Overlay Service*. Paris, France, European Space Agency.
- EUROCONTROL. (2010). *UAS C3 Channel Saturation Study Final Report*. Technical Report, EUROCONTROL.
- EUROCONTROL/FAA. (2007). *Action Plan 17 Future Communications Study, Final Conclusions and Recommendations Report*. Technical Report, EUROCONTROL / FAA.
- Hernandez-Pajares, M., Zornoza, J. M. J. and Sanz, J. S. (2005). *GPS Data Processing: Code and Phase Algorithms, Techniques and Recipes*. University Politecnica de Catalunya, Barcelona, Spain.
- Howell, C. T., Jessup, A., Jones, F., Joyce, C., Sugden, P., Verstynen, H. and Mielnik, J. (2010). The NASA Langley Research Center's Unmanned Aerial System Surrogate Research Aircraft. *Proceedings of Digital Avionics Systems Conference (DASC), 2010 IEEE/AIAA 29th*, Salt Lake City, Utah, USA.
- ICAO. (2008). *Performance-based Navigation (PBN) Manual*. International Civil Aviation Organization, third edition, Montreal, Quebec, Canada.
- Kamali, B. (2010). An Overview of VHF Civil Radio Network and The Resolution Of Spectrum Depletion. *Proceedings of Integrated Communications Navigation and Surveillance Conference (ICNS)*, Herndon, VA, USA.
- Kerczewski, R. and Kraft, T. (2006). The Future of Required Total System Performance RTSP. *Proceedings of Integrated Communications Navigation and Surveillance Conference (ICNS)*, Herndon, VA, USA.
- Kozco, S. (2010). Overview of NextGen ICNS Functional Requirements. *Proceedings of Integrated Communications Navigation and Surveillance Conference (ICNS)*, Herndon, VA, USA.
- Langley, R. B (1999). Dilution of Precision. *GPS World*, **1**, 52–59.
- Palmer, D., Moore, T., Hill, Ch., Andreotti, M. and Park, D. (2011). Radio Positioning Using the Digital Audio Broadcasting (DAB) Signal. *The Journal of Navigation*, **64**, 45–59.
- Parkinson, B. W. and Spilker, J. J. Jr. (1996). *Global Positioning System: Theory and Applications*. American Institute of Aeronautics and Astronautics.
- Qu, Y. and Zhang, Y. (2011). Cooperative Localization Against GPS Signal Loss in Multiple UAVs Flight. *Journal of Systems Engineering and Electronics*, **22**, 103–112.
- RTCA. (2006). Minimum Operational Performance Standards for Global Positioning System / Wide Area Augmentation System Airborne Equipment. Technical Report, RTCA.
- Schnell, M., Franzen, N. and Gligorevic, S. (2010). L-DACS1 Laboratory Demonstrator Development and Compatibility Measurement Set-Up. *Proceedings of Digital Avionics Systems Conference (DASC), 2010 IEEE/AIAA 29th*, Salt Lake City, Utah, USA.
- Stroup, R. L., Schaffer, G., Whittaker, J. and Niewoehner, K. (2010). Nextgen Air-Ground Integration Challenges. *Proceedings of Integrated Communications Navigation and Surveillance Conference (ICNS)*, Herndon, VA, USA.
- Symmetricom, (2009). XLI Time and Frequency System.
- Volpe, J. A. (2001). *Vulnerability Assessment of the Transportation Infrastructure Relying on the Global Positioning System*. National Transportation Systems Center Technical Report, Washington, DC, USA.
- Welch, G. and Bishop, G. (2001). *An Introduction to the Kalman Filter*. Los Angeles, California, USA.